Journal of Membrane Science 711 (2024) 123162

Contents lists available at ScienceDirect

Journal of Membrane Science

journal homepage: www.elsevier.com/locate/memsci

Spray coating of 2D materials in the production of antifouling membranes for membrane distillation

Clara Skuse [a], Monica Alberto [a], José Miguel Luque-Alled [b,c], Vicente Orts Mercadillo [d], Edidiong Asuquo [a], Alejandro Gallego-Schmid [e], Adisa Azapagic [a], Patricia Gorgojo [a,b,c,*]

[a] Department of Chemical Engineering, The University of Manchester, Manchester, M13 9PL, United Kingdom
[b] Instituto de Nanociencia y Materiales de Aragón (INMA), CSIC-Universidad de Zaragoza, Zaragoza, 50018, Spain
[c] Departamento de Ingeniería Química y Tecnologías del Medio Ambiente, Universidad de Zaragoza, Zaragoza, 50018, Spain
[d] National Graphene Institute, School of Engineering, The University of Manchester, Manchester, M13 9PL, United Kingdom
[e] Tyndall Centre for Climate Change Research, Department of Civil Engineering and Management, The University of Manchester, Manchester, M13 9PL, United Kingdom

ARTICLE INFO

Keywords:
Membrane distillation
Spray coating
Water treatment
Graphene oxide
Membrane scale-up

ABSTRACT

Membrane surface coatings with 2D materials have been shown to exhibit antifouling properties for water-treatment applications; however, synthesis methods currently based on vacuum filtration are not easily scalable. This study describes a scalable method for coating membranes with a range of 2D materials including graphene oxide (GO), hexagonal boron nitride (hBN), molybdenum disulphide (MoS_2) and tungsten disulphide (WS_2). Isopropyl alcohol solutions containing each class of the 2D flakes were spray-coated onto commercial polyvinylidene fluoride (PVDF) using a pyrolyser. The nanomaterials were secured with polydopamine (PDA) as a crosslinker in a method that could easily be integrated into a scalable roll-to-roll process. Changes in morphology, surface roughness, hydrophobicity, mechanical durability and chemical composition were evaluated using scanning electron microscopy, atomic force microscopy, contact angle, tensile strength measurements and Fourier-transform infrared spectroscopy. The 2D nanomaterials-coated membranes were tested in membrane distillation (MD) experiments over 72 h and compared to pristine PVDF and PDA/PVDF membranes. Salt rejection and MD performance stability were evaluated using feedwaters with high concentrations of humic acid (150 ppm) and paraffin oil (200 ppm) simulating simple organic wastewater from oil and gas extraction. The flux decline ratio was measured in terms of percentage permeate loss per hour (%/h), to allow for future comparisons with studies with different experimental times. The pristine PVDF membrane failed after 10 h by pore-wetting due to fouling while the PDA/PVDF membrane had the largest flux decline ratio (0.3 %/h). The membranes coated with GO and hBN had flux decline ratios orders of magnitude lower (0.0021 ± 0.005 and 0.028 ± 0.01 %/h, respectively). All membranes had a high salt rejection (>99.9 %). The GO-coated membrane was the only membrane type that was able to treat both surfactant-containing and foulant-containing feedwaters. The improved performance is attributed to the decrease in both surface roughness and hydrophobicity, which reduces the adsorption of foulants onto the membrane surface. This work shows a facile, scalable method to overcome fouling limitations in MD.

1. Introduction

As access to freshwater sources is becoming more difficult in many regions, it is increasingly important to improve the way we manage and produce potable water. One way to achieve this is to increase the production of water from unconventional sources, such as wastewater. Membrane-based technologies are well established and widely used for water treatment due to their high selectivity, lower energy consumption, compactness and scalability when compared with chemical- and distillation-based technologies [1]. Wastewaters are typically difficult to treat as they contain high amounts of organic compounds and surfactants, the latter of which causes pore wetting in membrane distillation (MD) [2]. Organic compounds are a particular problem as they deposit onto the membrane surface, subsequently blocking the pores and causing a decline in the permeate flux. This phenomenon is called fouling and it is considered one of the largest issues for membrane-based

* Corresponding author. Departamento de Ingeniería Química y Tecnologías del Medio Ambiente, Universidad de Zaragoza, Zaragoza, 50018, Spain.
E-mail address: pgorgojo@unizar.es (P. Gorgojo).

https://doi.org/10.1016/j.memsci.2024.123162
Received 1 May 2024; Received in revised form 30 July 2024; Accepted 2 August 2024
Available online 5 August 2024

water treatment technologies.

MD is being explored as an alternative and complementary method for water treatment due to some advantages over conventional membrane-based methods, such as reverse osmosis (RO). For example, in MD the energy consumption does not depend on the feed concentration; thus, it can treat highly saline, foulant-containing solutions. In particular, MD is being investigated for the purification of wastewater that RO cannot currently treat [3,4]. While MD has a lower fouling propensity when compared to RO, there is still a limit as to what membranes can feasibly separate [5]. For example, solutions containing 160 ppm of organic foulants or 100 ppm of oils can cause a significant (>30 %) reduction in the permeate flux, as well as wetting of the membrane [3,6]. Even solutions with concentrations as low as 10 ppm of humic acid and 10 ppm of paraffin oil have exhibited flux decline and pore wetting in MD [7].

The key to unlocking wastewater as a source of potable water is the development of antifouling, antiwetting, long-lasting membranes with high selectivity and permeability. One of the major advantages of MD over conventional RO is that it can achieve high rejections of solutes [8,9]. However, a recent study has suggested that trace amounts of non-volatile humic acid can penetrate through MD membranes due to hydrophobic attractions between the organic compound and the membrane [10]. Thus, it is important to further investigate whether this phenomenon can be controlled. In our work we have explored the use of a range of 2D materials for improved pore wetting and anti-fouling resistance.

2D materials, such as graphene [11], graphene oxide (GO) [12], molybdenum disulphide (MoS_2) [13], tungsten disulphide (WS_2) and hexagonal boron nitride (hBN), are being explored to overcome issues within the field of membrane separation. Studies on the effects of 2D materials on membrane fouling within MD are extremely limited, thus pressure-driven processes are discussed in the sections below. Graphene is a 2D material composed of sp^2-hybridised carbon atoms arranged in a hexagonal lattice. Its discovery was well received due to the extensive list of desirable properties, such as high mechanical strength [14,15], electrical conductivity [16], thermal conductivity [17] and functionalisation capabilities [18]. Graphene oxide (GO) is a derivative of graphene which can be dispersed easily in water and most organic solvents [19,20]. Alternatively, GO flakes can be stacked together to form a laminate membrane with excellent molecular sieving capabilities [21]. The spacing between each GO flake (i.e. the d-spacing) is 0.83 nm, which is large enough for water to pass through and small enough to stop hydrated solutes [22]. Studies show that under these confinement conditions, water molecules traverse through the membrane with unimpeded motion [20,21]. The nano-pores provide a high capillary force, which is the main driving force that draws water inside the GO membrane. The high capillary force and unimpeded motion give rise to high flux membranes, which are ideal for water treatment applications [23,24].

MoS_2 and WS_2 are also 2D materials which belong to the transition-metal dichalcogenide (TMD) group of type MX_2, whereby M is a transition metal and X is a chalcogen atom [25] and are considered in this work. To the best of our knowledge, this is the first study so far investigating the use of MoS_2 membranes for MD. Other authors have considered MoS_2 but for different applications. For example, Koh & Taek [13] fabricated a MoS_2-PVDF composite membrane for the removal of ethylene glycol. The addition of MoS_2 produced a more omniphobic membrane that had a water flux of 27 L/m^2 h, but this decreased to 21 L/m^2 h after 8 h. The addition of MoS_2 as a coating is relatively unexplored, even throughout commercialised water treatment technologies [26]. There are molecular dynamic studies on laminate MoS_2, which claim rapid water transport properties and high salt rejection, but lack experimental studies [27]. Overall the results from these preliminary experiments and molecular dynamic simulations suggest that TMDs, like MoS_2 and WS_2, could have significant antifouling, high permeability and anti-wetting properties.

Similarly, molecular dynamic studies indicate that laminate hBN membranes can have high permeability and ion rejection [28]; the polar B–N bonds in hBN have a high affinity with water, which can selectively transport water through the hBN nanochannels. Also, hBN coatings can increase membrane hydrophobicity and lead to long-term MD stability [29]. Several studies have shown that using hBN as a polymer additive can also increase permeability [30,31], and pore wetting resistance [32].

For water treatment, these materials have been extensively explored as nanofillers to form composite mixed matrix membranes (MMMs) [33,34]. While GO certainly has the largest share of research, molecular dynamic simulations suggest that MoS_2, hBN and WS_2 could have even greater molecular sieving capabilities than GO [35,36]. There are fewer studies on the antifouling properties of these materials [37–42] and even fewer on their application in MD [43,44].

In contrast to MMMs, there are not as many studies using these materials for laminate membranes and surface coatings; this is partially due to poor flake adhesion and swelling, which limit commercial viability [45]. Studies have investigated cross-linkers to help immobilise the 2D laminate layer. Some of these cross-linkers include metal ions, such as TiO_2 [46], polydopamine (PDA) [47,48], and polyphenols, such as tannic acid [49]. In our previous study [50], we demonstrated the use of bio-sourced polydopamine (PDA) as an immobiliser to fix the GO flakes to the surface of the hydrophobic polyvinylidene fluoride (PVDF), without affecting the flux.

Laminate membranes have been explored for ultra-fast water permeation, including for GO [51], MoS_2 [13,35], hBN [52] and WS_2 [36,53]. However, the operating conditions differ greatly from study to study, making comparisons between the performance of the different materials nearly impossible. Further, vacuum filtration is used extensively throughout 2D membrane research to deposit flakes into an ordered laminate membrane, but scalability is a major issue as it cannot be easily integrated into a roll-to-roll process. Other coating methods, such as dip-coating and drop-casting, are scalable, but controlling the laminate thickness and flake orientation is challenging [54]. Electrospraying has shown to deposit GO flakes on nanofiltration membranes, as described in a study by Chen et al. [55]. The resulting membrane had a high rejection of organic dyes (98.88–100 %), but a poor rejection of salts (27.9 % NaCl rejection and 41.8 % $MgSO_4$ for a 0.02 M feed solution). In comparison, typical commercial nanofiltration membranes have a NaCl and $MgSO_4$ rejection of 20–80 % and 90–98 %, respectively. A reason for the low rejection using this fabrication method could be improper immobilisation of the GO flakes, leading to swelling. The electrospraying process also requires careful selection of a carrier solvent to form the spray cone; for the deposition of nanomaterials, solvents such as N-methyl-2-pyrrolidone (NMP) and dimethyl sulfoxide (DMSO) are commonly used [56]. Thin-film deposition via electrospraying is usually paired with pyrolysis to speed up the rate of solvent evaporation [57]. Spray pyrolysis has been described as a facile, effective and suitable method for industrial scale-up fabrication of nanostructured materials for energy storage devices [58–60]. However, as far as the authors are aware, this technology has not been solely applied for the production of 2D-enhanced membranes, or for water treatment.

To address some of the above issues, this study advances upon previous work by describing an inherently highly scalable production method appropriate for industrial commercialisation – a 1 step-spray-coating technique – for the deposition of 2D flakes onto membranes. Four 2D materials were considered for these purposes: GO, MoS_2, hBN, and WS_2. The membranes enhanced with these materials ("2D-enhanced membranes") were evaluated in terms of permeate flux, rejection and fouling performance for feed solutions containing mineral oil (paraffin oil was used in these experiments) and humic acid. These materials were selected in order to evaluate both oil and organic fouling in MD [61] and they simulate simple oily wastewater [62].

2. Methods

2.1. Materials

Graphene oxide (GO) was purchased from William Blythe Ltd (UK). Dopamine hydrochloride (DA, 99 %), tris(hydroxymethyl)aminomethane (Tris-HCl, pH = 8.5, 0.5 M) and isopropyl alcohol (IPA, ≥99.7 %) were purchased from WWR International (UK). Commercial PVDF membranes were purchased with a nominal pore size of 0.22 μm and average thickness of 125 μm (GVHP09050). Ethanol (≥99.0 %) and sodium chloride (NaCl, ≥99.0 %) were purchased from Merck Life Science UK Ltd (UK). Paraffin oil was purchased from VWR chemical and humic acid was purchased from Merck Life Science Ltd. Hexagonal boron nitride (Hexotene) was purchased from Versarien. MoS_2 and WS_2 powder was purchased from Sigma Aldrich (<2 μm, 98 % and <2 μm, 99 %, respectively).

2.2. Fabrication of transition metal dichalcogenides

MoS_2 powder was exfoliated using 1g of commercial MoS_2 powder in a 500 ml IPA/H_2O solution (50:50) at a concentration of 2 mg/ml under the assistance of ultrasonication for 24 h at a frequency of 37 Hz and 40 % power with an Elmasonic P sonicator. A Julabo-F250 chiller was used to maintain the temperature at 15 °C. The resulting product was then centrifuged twice using an Eppendorf 5804R refrigerated centrifuge at 6500 rpm at 20 °C for 30 min to remove the non-exfoliated MoS_2. The exfoliated MoS_2 dispersion was extracted from the supernatant with a narrow distribution of flake dimensions and thicknesses, as reported elsewhere [35]. WS_2 powder was also exfoliated using the protocol described above.

2.3. Membrane preparation

The 2D materials were encased on both sides by a PDA coating to reduce delamination and leaching into the aqueous feed solutions. More details on the PDA synthesis can be found in our previous work [50]. After the deposition of the first PDA layer, the membranes were spray-coated with an IPA solution containing the 2D material using a Spray Pyrolyser HO-TH-04 as shown in Fig. 1. The 2D materials were dispersed into IPA and sonicated for 30 min immediately before spray coating. The IPA/2D solution added to the pyrolysis machine had a concentration of 0.04 mg/mL, the hot plate was set to 120 °C and the coating was applied at 8000 μl/min for 120 s over an area of 10 cm × 10 cm. Lastly, the final coating of PDA was applied using the same procedure outlined in our previous work [50]. The spray pyrolysis stage could be a continuous flow procedure by the addition of a roll-to-roll system (as outlined by the equipment manufacturers), which shows the potential for mass production.

The four types of membrane are denoted GO-PDA/PVDF, hBN-PDA/PVDF, MoS_2-PDA/PVDF and WS_2-PDA/PVDF. The pristine commercial membrane is denoted PVDF and the control membrane is PDA/PVDF which had two coats of PDA and was heated for the same time period.

2.4. Membrane distillation set-up

Firstly, the membranes were cut into circles with an area of 9.1 cm^2 and installed into an air-gap MD (AGMD) system as shown in Fig. 2. Three membranes were tested of each type (GO, hBN, MoS_2 and WS_2) to assess reproducibility, and fouling and pore-wetting experiments were conducted for each membrane type. From the beginning of the experiment, the feed solution contained 150 ppm humic acid and 200 ppm paraffin oil, which is the upper range considered in literature for MD organic and mineral oil fouling [3,6,7,63]. The humic acid and paraffin oil were sonicated for 5 min and the solution was added to 1L of 35.5 g/L

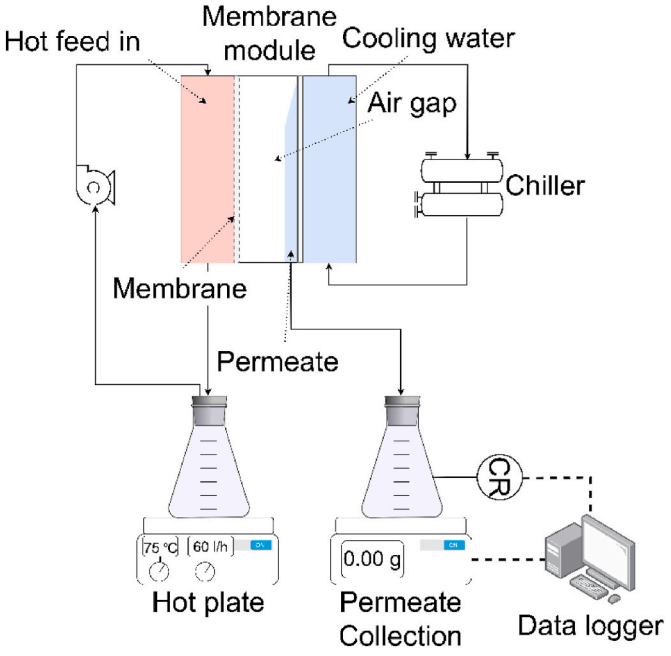

Fig. 2. Schematic diagram of the membrane distillation set up (CR: conductivity recorder).

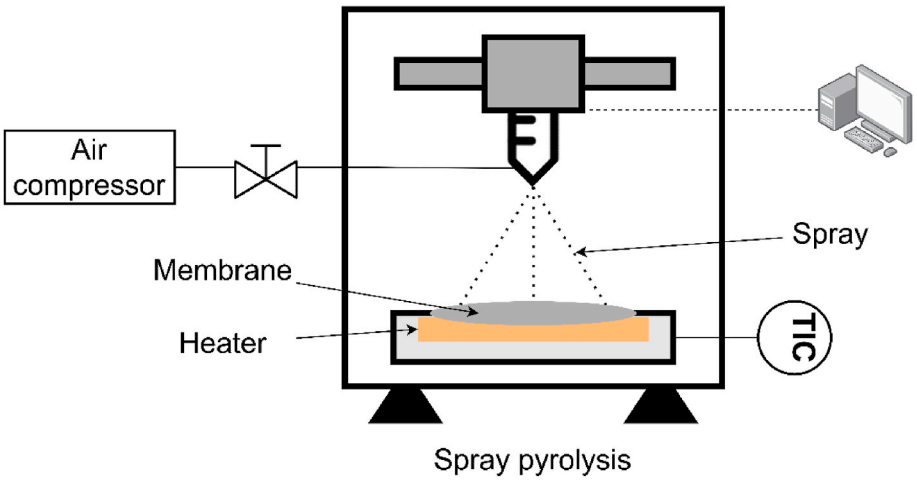

Fig. 1. Schematic diagram of the spray pyrolysis machine coating a membrane (TIC: temperature indicator controller).

NaCl aqueous solution. The feed solution was stirred continuously for the duration of the experiments and no phase separation was observed during testing. The feed solution was heated to 75 °C and was recirculated through the feed side of the membrane cell with a flow rate of 60 L/h for the entire experiment. The condenser plate was kept cool using cooling water that was circulated from the chiller unit set at 20 °C. For all experiments, the membrane was operated for 1 h before collecting data, to ensure the system was at steady state. The mass of permeate was recorded every 30 min and the permeate flux was calculated using Equation (1):

$$J = \frac{\Delta m_p}{A \Delta t} \quad \text{(Eq. 1)}$$

where J is the flux (kg/m^2 h), Δm_p is the change in the permeate mass (kg) over time period Δt (h), and A is the effective membrane area (m^2). The collected permeate was regularly added back into the feed solution to ensure continuous operation.

The salt rejection (SR) indicates if pore wetting has occurred, and it is calculated using Equation (2):

$$SR = \left(1 - \frac{C_p}{C_f}\right) \times 100\ \% \quad \text{(Eq. 2)}$$

where SR is given in %, and C_p and C_f are the conductivity of the permeate and feed, respectively (μS/cm). The conductivity was recorded every 10 min using a Go Direct™ conductivity probe.

The flux decline ratio (FDR) shows the level of fouling and it was calculated according to Equation (3):

$$\text{FDR} = \left(\frac{J_{p,i} - J_{p,f}}{J_{p,i}}\right) \times 100 \Big/ t \quad \text{(Eq. 3)}$$

where J_p is the permeate flux (L/m^2 h) at the initial (i) and final (f) experimental time t (h). The flux values were plotted and the best-fit equation used to calculate the FDR. The initial flux was taken as the y-intercept of the trendline and the final flux was calculated using the linear equation. In this study, the FDR was expressed in %/h to enable comparisons with studies that have different experiment times.

2.5. 2D-material and membrane characterisation

Scanning electron microscopy (SEM) was used to determine the lateral size distribution of the 2D materials. Specimens were prepared by immersing pieces of a silicon dioxide wafer (thickness 290 nm) into the different IPA-based dispersions and left to dry at 50 °C. The samples were then imaged using a Quanta 250 FEG-SEM (FEI, USA) with a voltage of 5 kV. Additionally, the thickness and surface morphology of the 2D nanosheets was assessed using atomic force microscopy (AFM) [64]. Samples were prepared by drop-casting 50 μl of a 100 ppm dispersion of 2D material (GO, hBN, MoS_2 and WS_2) onto mica substrates for 2 min. After this, excess solution was wicked from the surface and the mica substrate was then rinsed ten times with 100 μl of double-distilled water. The excess solution was removed and the samples were left to dry overnight. Samples were imaged in the air under ScanAsystTM mode with a Bruker Multimode 8 system, a Nanoscope V controller and a "J" scanner (Bruker Ltd., UK). For the flake analysis, ScanAsyst-Air probes were used with a nominal spring constant (k) of 0.4 N/m (Bruker AXS S.A.S, France) and the system was controlled via the Bruker Nanoscope software v8.15. At least ten images were taken per 2D material and all were first-order flattened prior to analysis using the Nanoscope Analysis software v1.40.

SEM and AFM were also used to characterise the morphology of the synthesised membranes. The AFM images were taken in the same way as for the flakes, except that the tapping probe NuNano Scout 350 (nominal frequency 350 kHz, spring constant 42 N/M, tip radius 10 nm) was used under the ScanAsystTM mode and all images were second-order flattened. The root-mean-square roughness was calculated using the Nanoscope Analysis software v1.40 from images of size 5 μm^2 and 500 nm^2 for the surface and localised roughness, respectively [65]. The average roughness was calculated by considering at least five images from different locations on the membrane.

Cross-sectional SEM specimens were prepared by cutting the membrane samples in liquid N_2 to obtain a cleaner section. Specimens were immersed in 0.5 % aqueous RuO_4 solution for 24 h to improve the image contrast. Further membrane coating with Pd (14 nm of thickness) was carried out to ensure sample electrical conductivity. All SEM specimens were imaged using an FEI-Inspect F20 microscope operating at 10–30 kW. Energy dispersive spectroscopy (EDS) was used for elemental analysis on membrane samples (without Pd coating). The samples were analyzed using a QUANTAX XFlash EDX Detector (Bruker, France).

X-ray photoelectron spectroscopy (XPS) measurements were carried out on a thin film of MoS_2 to assess whether changes in chemical composition occurred after heat treatment at 120 °C. The film was prepared on a PDA-coated PVDF support by vacuum filtration of 4 mL of a 2 mg/mL MoS_2 dispersion in IPA/H_2O and half of it was placed on a hot plate and heated from room temperature to 120 °C. The samples were dried in a vacuum oven at 60 °C for 12 h prior to analysis. A Kratos Axis Ultra spectrometer with a monochromatic Al Kα X-ray source (1486.6 eV) at 10 mA, 15 kV and 150 W power was used. Spectra were analyzed using CasaXPS software.

To measure the contact angle of the membranes, a DSA100B Drop Shape Analyser (KRUSS, Germany) was used. The angle was calculated using the sessile drop method with a 10 μL drop size of deionised water. The average values resulted from the water contact angles from at least five different locations on the membrane. Membranes were glued on a flat glass slide with double-sided tape.

Immobilisation of the 2D flakes onto the membrane surface was evaluated by measuring detachment via a Genesys 10 S UV–Vis spectrophotometer (Thermo Scientific, UK), using a quartz cuvette with a 1 cm optical path at room temperature. Membranes were cut into 28 mm-sized circles and placed in 8 ml of deionised water while agitated using IKA-VIBRAX-VXR for two weeks at room temperature. Detachment was calculated in terms of mg of 2D material that detaches in water per m^2 of membrane. The water that had contacted the membrane was then tested and the concentration of 2D material was measured using UV.

The Fourier transform infrared spectroscopy (FTIR) spectra was measured for the GO-PDA/PVDF, hBN-PDA/PVDF, MoS_2-PDA/PVDF and WS_2-PDA/PVDF membranes, as well as their respective 2D powders. This was performed using a VERTEX 70V FT-IR spectrometer (Bruker, USA) in the range 500–4000 cm^{-1} with a scanning rate of 1 cm^{-1}.

X-ray diffraction (XRD) was carried out in a Bruker D8 Discover GIXRD Autochanger instrument with a Cu X-ray source with a total scan time of 30 min per sample and a 2Θ range of 5–80°.

A Static Testing Instron 5564 H 1580 machine using a 10 N load was used to investigate the mechanical properties of the membranes. The tensile strength is the maximum load that the membrane can support without fracture when being stretched, indicating the durability of the membranes. The membranes were cut to widths of 5 mm and the length of the strip was 25 mm. The speed was set to 25 mm/min and the stress-strain curve was recorded to measure the maximum tensile strength. Five samples were taken per membrane type to assess reproducibility.

3. Results and discussion

3.1. 2D-material characterisation

The lateral size of the 2D flakes was measured by analysing over 100 flakes from the SEM images for each material (see Figs. 3 and 4) and the mean values were as follows: GO: 1.9 ± 1.7 μm; hBN: 2.0 ± 2.1 μm; MoS_2: 0.43 ± 0.5 μm; and WS_2: 1.5 ± 1.2 μm. AFM was used to determine the agglomeration of the flakes by measuring the thickness. The average thickness measured across at least 25 flakes per sample was as

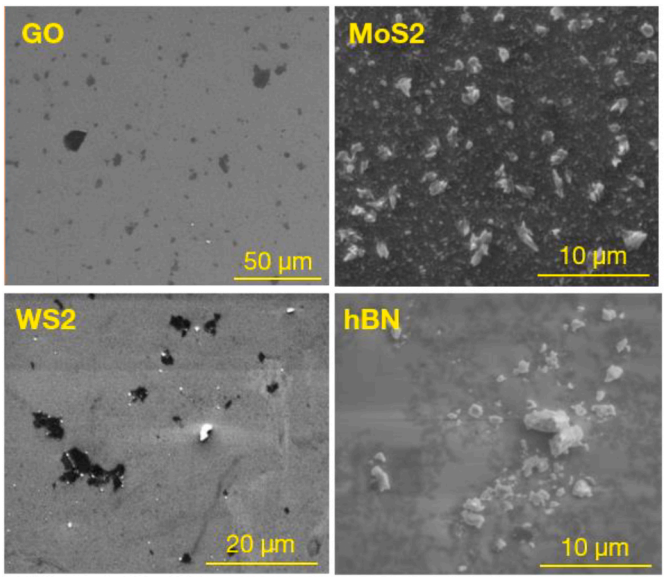

Fig. 3. Scanning electron microscope images of the graphene oxide (GO), hexagonal boron nitride (hBN), molybdenum disulphide (MoS_2) and tungsten disulphide (WS_2) flakes.

follows: GO: 0.9 ± 0.6 nm; hBN: 3.4 ± 1.1 nm; MoS_2: 2.4 ± 1.5 nm; and WS_2: 2.1 ± 0.9 nm. The AFM flake images can be found in Fig. S1 in the Supplementary Information (SI).

3.2. Membrane characterisation

Fig. 5 shows AFM 3D surface images for the commercial PVDF substrate before and after PDA deposition, and membranes onto which the selected 2D materials (GO, hBN, MoS_2 and WS_2) were deposited. The AFM images of 5 × 5 μm sample areas suggest a homogeneous deposition of the GO flakes onto the PVDF with a smooth and continuous coverage of the surface. This is also evident from the root-mean-square (Rq) roughness values (Table 1); as a result of the GO deposition, the membrane surface roughness is reduced by 45–48 % when compared to the PDA and PVDF membranes, having also a narrower spread of values. A good degree of coverage is obtained also with hBN and WS_2 (Rq is reduced by 54 % and 43 %, respectively, when compared to the commercial PVDF) and a smaller roughness reduction for the MoS_2 coated membrane (29 %).

The cross-sectional SEM images (Fig. 6) do not display a clear layer of the 2D materials due to poor contrast between the porous PVDF substrate and the 2D films that are sandwiched in between PDA. Considering no loss of material in the pyrolyser chamber during spray deposition, and literature values of density for the 2D materials (0.981 g/cm^3 (GO) < 2.1 g/cm^3 (hBN) < 5.06 g/cm^3 (MoS_2) < 7.5 g/cm^3 (WS_2)), theoretical coating thicknesses are 652 nm (GO) > 305 nm (hBN) > 126 nm (MoS_2) > 85 nm (WS_2). Fig. 7a is a Raman map displaying the deposition of GO flakes onto the membrane surface. The distinctive peaks in the Raman spectra in Fig. 7b seen at wavenumbers ~1300 cm^{-1} and ~1500 cm^{-1} correspond to the D and G peaks; these values agree with the literature for Raman spectra for GO and suggests that there is deposition of GO on the membrane surface [66]. The deposition of 2D flakes onto the polymeric membrane support was also confirmed with Raman for the hBN-PDA/PVDF, MoS_2-PDA/PVDF and WS_2-PDA/PVDF; the spectra in Fig. 8 shows the E_{2g} optical phonon peaks at 1362, 383 and 356 cm^{-1} respectively, which agrees with literature [67,68]. Further evidence for the deposition of hBN, MoS_2 and WS_2 onto the polymer surface can be seen in the EDS results in Fig. S2. For the hBN-PDA/PVDF membrane, the EDS analysis showed peaks for the elements boron and nitrogen, as well as peaks for carbon and fluorine that derive from the PVDF membrane. Similar trends can be seen for the MoS_2-PDA/PVDF and WS_2-PDA/PVDF membranes. The conditions during spray coating (120 °C) were below the recorded temperatures and exposure times that cause thermal decomposition in monolayer GO [69], hBN [70], MoS_2 [71] and WS_2 [72]. XPS results on MoS_2 films before and after the heat treatment at 120 °C confirmed no changes in their chemical structure (the C 1s, O 1s, Mo 3d, and S 2p spectra are shown in Fig. S3).

The addition of the PDA reduced the contact angle from 118° to 101°, as the material is hydrophilic. Values can be found in Table 1. The addition of GO, hBN and MoS_2 also reduced the contact angle further to 75.4°, 83.4° and 85.2°. However, the addition of WS_2 increased the contact angle slightly to 108.8° due to its hydrophobicity [73]. Increasing membrane hydrophilicity has shown to enhance membrane

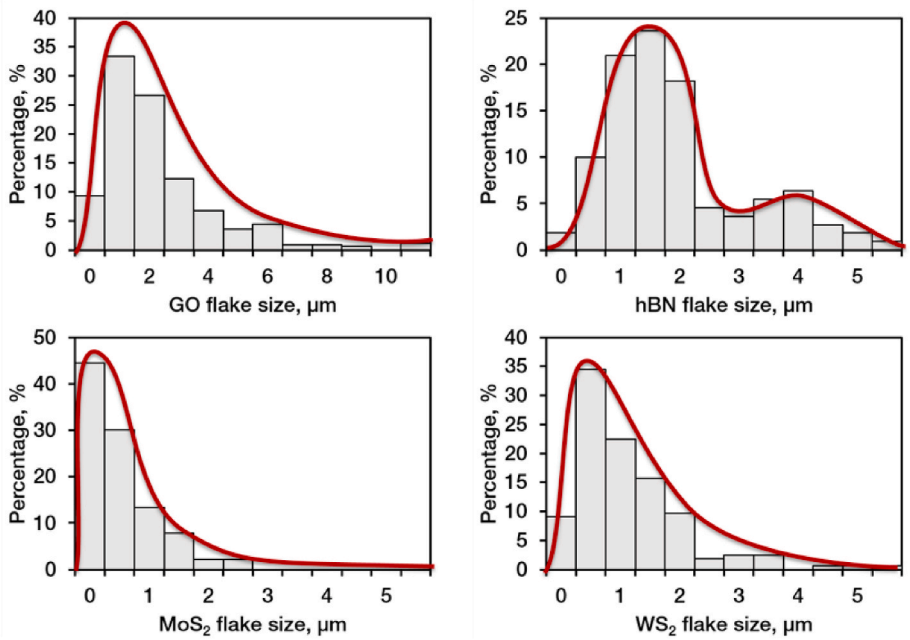

Fig. 4. Flake size analysis for graphene oxide (GO), hexagonal boron nitride (hBN), molybdenum disulphide (MoS_2) and tungsten disulphide (WS_2).

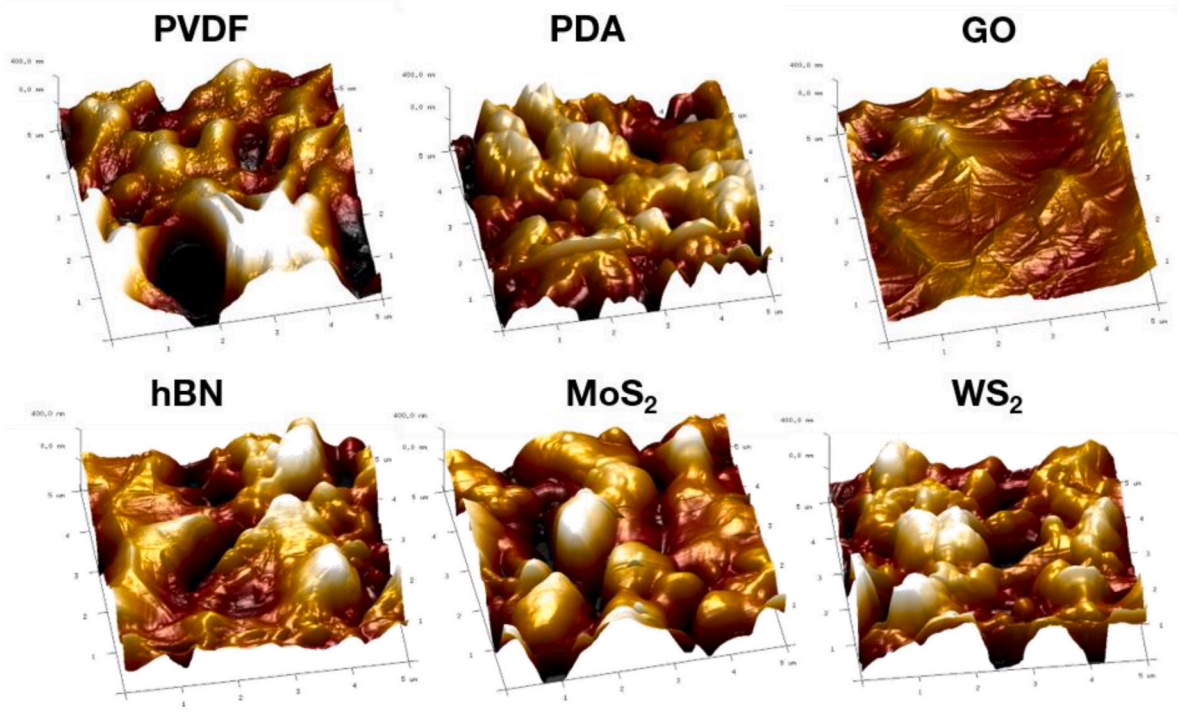

Fig. 5. AFM surface images of the PVDF, PDA-PVDF, GO-PDA/PVDF, hBN-PDA/PVDF, MoS_2-PDA/PVDF and WS_2-PDA/PVDF membranes.

Table 1
Overview of the membrane properties including the root-mean-square roughness (Rq), tensile strength, tensile strain, and contact angle measurements before and after the fouling experiments.

Membrane ID[a]	Roughness (R_q), nm	Tensile strength, MPa	Tensile strain, %	Contact angle, °	
				Before	After
PVDF	322 ± 105	7.0 ± 0.2	51.1	118 ± 4	105 ± 2
PDA/PVDF	301 ± 139	5.0 ± 0.2	50.1	101 ± 2	46 ± 7
GO-PDA/PVDF	167 ± 68	5.0 ± 0.5	41.3	75 ± 1	31 ± 6
hBN-PDA/PVDF	149 ± 54	7.0 ± 0.5	68.8	83 ± 1	24 ± 11
MoS_2-PDA/PVDF	230 ± 75	7.0 ± 0.4	58.4	85 ± 6	54 ± 13
WS_2-PDA/PVDF	182 ± 23	8.0 ± 0.6	61.8	109 ± 4	51 ± 6

[a] Polyvinylidene fluoride (PVDF), polydopamine (PDA), graphene oxide (GO), hexagonal boron nitride (hBN), molybdenum disulphide (MoS_2) and tungsten disulphide (WS_2).

antifouling properties but reduce the liquid entry pressure [74]. While increasing the membrane hydrophobicity may improve antiwetting properties, interactions between hydrophobic foulants and the hydrophobic membrane can increase the fouling propensity [75]. Thus, the hydrophobicity/hydrophilicity of the membrane is not sufficient to determine whether the membrane exhibits the desired properties for an antiwetting/antifouling membrane. Surface roughness is a superior indicator of antiwetting and antifouling behaviour [76].

Immobilisation of the 2D materials was determined by UV–Vis spectroscopy and the calibration curves can be found in Fig. S4. The absorption peaks were 231 nm for GO, 203 nm for hBN, 399 nm for MoS_2 and 639 nm for WS_2, in agreement with values reported in the literature [77–80]. The cause of the absorption peak for GO is attributed to the π-π* plasmon peak caused by the conjugative effect of chromophore aggregation. The amount of 2D material in the water after two weeks was 3.69 mg/m^2, 19.8 mg/m^2, 9.14 mg/m^2 and 21.4 mg/m^2 for GO, hBN, MoS_2 and WS_2, respectively. In terms of material percentage loss, this equates to 5.7 % for GO, 30.9 % for hBN, 14.3 % for MoS_2 and 33.4 % for WS_2 if we consider an initial coverage of 64 mg of 2D flakes per m^2 of the spray coated membranes (assuming no loss of 2D materials in the pyrolyser chamber). Figures of detachment for the GO-coated membranes do not suggest concerns, however pre-treatment of the membranes where the 2D materials could be recovered is suggested to minimise leakage into the aqueous feed solutions during operation.

The FTIR and XRD spectra for each of the 2D powders and their respective membranes can be seen in Figure S5 and Figure S6, respectively. The membrane FTIR spectra shows strong peaks at 873 cm^{-1} and 1072 cm^{-1}, which correspond to the in-phase symmetric stretching of CF_2 and the symmetric phase II stretching of the C–C bonds in the PVDF, respectively. The FTIR spectra for PVDF and PDA is identical, suggesting that the PVDF masks the signal from the PDA, and this is seen by the absence of some individual peaks from the 2D materials. However, for the MoS_2 and WS_2 membranes there is a an additional peak at 1217 cm^{-1} and a splitting of the 1179 cm^{-1} peak due to the presence of S–S and S═O bonds, respectively [81]. The S═O bonds are present due to partial oxidation during MoS_2 and WS_2 synthesis. The XRD graphs show similar behaviour and the distinct peaks from the 2D materials are not visible in the membrane spectra. This could be due to the PVDF membrane sample being too thick during analysis, as the concentration of nanomaterials on the surface is significantly lower than the PVDF.

The mechanical properties of the membranes are shown in Table 1. It can be observed that the addition of PDA reduced the tensile strength by 28 % when compared to the pristine PVDF, decreasing from 7 to 5 MPa. This could be due attributed either to the PDA layer or the heat

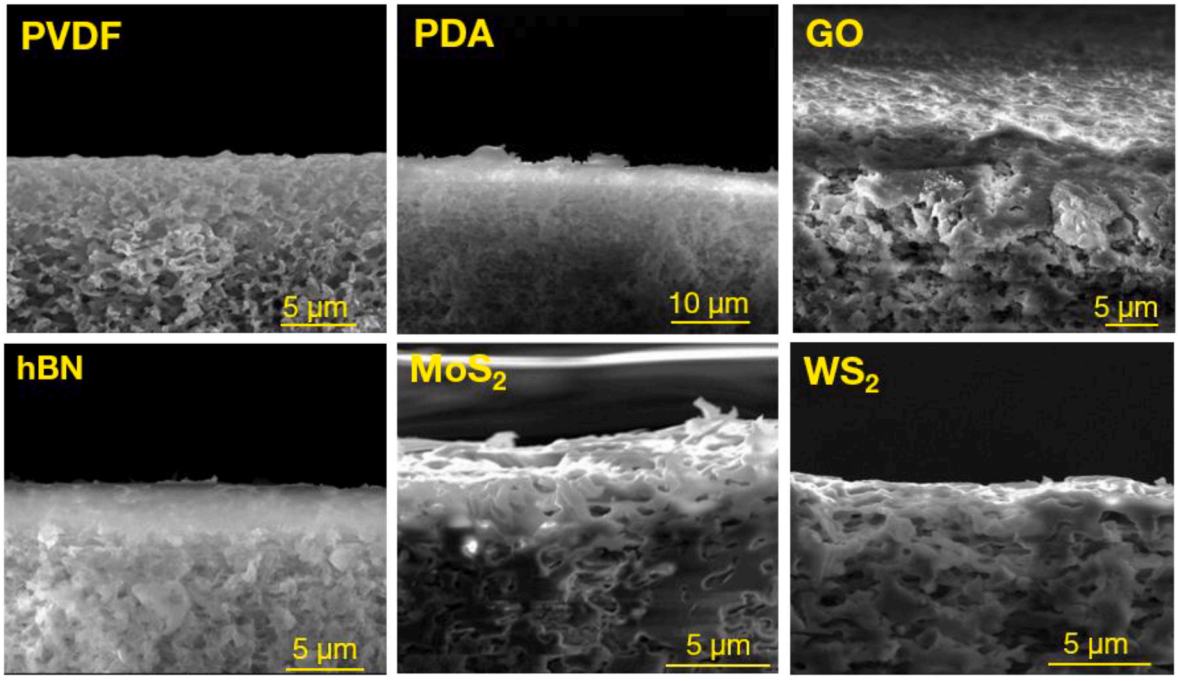

Fig. 6. Cross-sectional scanning electron microscopy images of the PVDF, PDA-PVDF, GO-PDA/PVDF, hBN-PDA/PVDF, MoS_2-PDA/PVDF and WS_2-PDA/PVDF membranes.

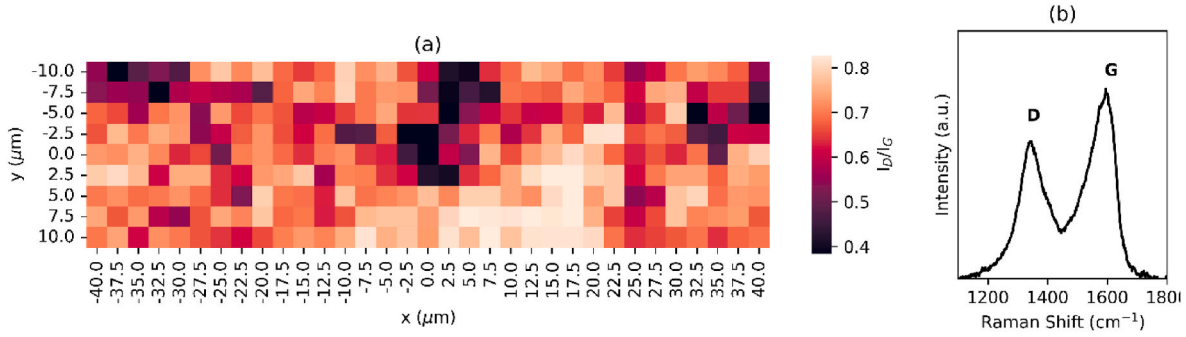

Fig. 7. (a) mapping of the graphene oxide (GO) thin film distribution (red/white) over the PDA/PVDF membrane (black) and (b) Raman spectra of the GO membrane. I_D and I_G correspond to the intensity of the D and G peaks, respectively. (For interpretation of the references to colour in this figure legend, the reader is referred to the Web version of this article.)

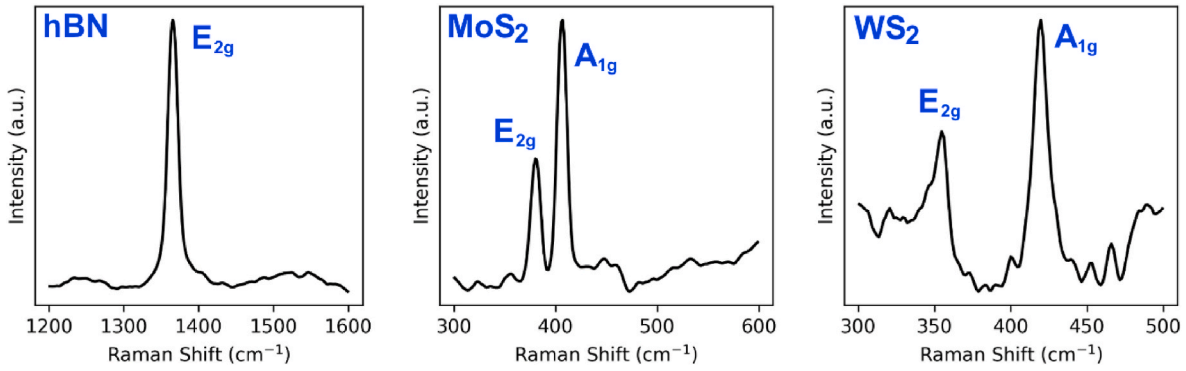

Fig. 8. (a) Raman spectra of hBN, MoS_2 and WS_2 membrane. E_{2g} and A_{1g} peaks refer to the in-plane vibration and out-of-plane mode respectively.

treatment at 120 °C during deposition. Furthermore, membranes prepared with 2D hBN and MoS_2 increased the maximum tensile stress up to the original value for untreated commercial PVDF substrates (7 MPa) and a bit further for WS_2 (8 MPa). All three deformed to a greater extent than the PDA/PVDF film. However, the deposition of GO reduced the tensile strain from 50.1 % to 41.3 % and did not have an effect on the tensile strength, that was also 5 MPa. Nevertheless, the mechanical properties of all the membranes in this work are comparable to those

reported in the literature for PVDF flat sheet membranes [82], and aging by mechanical stress in MD is a minor contributor in comparison to irrecoverable fouling, which is the leading reason for membrane replacement [5,6]. Thus, as the membrane is not exposed to high pressures, the slight reduction in tensile strength for the GO-PDA/PVDF membrane is not expected to be an issue.

3.3. Membrane fouling performance

The flux decline due to fouling was observed for each of the membranes as shown in Fig. 9. Raw conductivity data can be found in Fig. S7 in the SI. As mentioned earlier, these experiments started with the foulants already present in the feed solution. Each experiment was repeated twice more to obtain the standard deviation, which was used to form the error bars in Fig. 10.

The initial flux can be seen in Fig. 9 and is listed as follows: PVDF, 9.5 ± 0.16 L/m^2 h; PDA/PVDF, 11.5 ± 1.4 L/m^2 h; GO-PDA/PVDF, 10.2 ± 0.52 L/m^2 h, hBN-PDA/PVDF, 10.6 ± 0.44 L/m^2 h; MoS_2-PDA/PVDF, 10.9 ± 0.81 L/m^2 h and WS_2-PDA/PVDF 10.9 ± 0.66 L/m^2 h respectively. Critically, the addition of GO and hBN onto the membrane increased the resistance to fouling, since a stable permeate flux is observed for both membranes. However, membranes coated with MoS_2 and WS_2 did show a small decrease in flux over the MD experiments, similarly to that for the PDA-coated PVDF substrate. This is due to stronger interactions between the hydrophobic foulants and the surface of the membranes, resulting from higher surface roughness and contact angle values for the PVDF substrate and the MoS_2 and WS_2 membranes (Table 1).

It can be seen in Fig. 9 that the as-received PVDF membrane failed after just over 10 h, as the salt rejection fell below 98 %. This is due to the adsorption of foulants onto the membrane surface, which eventually reduced the surface tension to the point where pore wetting occurred. The increase in flux coincided with the reduction in the salt rejection and indicated the passage of feedwater. The salt rejection for the GO-PDA/PVDF, hBN-PDA/PVDF and WS_2-PDA/PVDF membranes was stable (>99.9 %) for the entire duration of the experiment (72 h). However, for the MoS_2-PDA/PVDF membranes, the salt rejection began to fail towards the end of the experiment. The stable high salt rejection for the GO-PDA/PVDF, hBN-PDA/PVDF and WS_2-PDA/PVDF 2D membranes and the PDA-coated PVDF substrate indicate good degree of coverage of the larger PVDF membrane pores that are responsible for pore wetting.

Fig. 10 shows the FDR values for the evaluated membranes; the pristine PVDF control membrane is not displayed as it failed before the end of the 72-h experiment. The PDA/PVDF control membrane showed resistance to pore wetting, which is demonstrated by the stable salt rejection (Fig. 9). Although the PVA/PVDF layer is resistant to fouling in the first 38 h of the experiment, there is a decline in flux for the remaining 34 h. Also, the FDR was the highest out of all of the experiments (0.30 %/h), which suggests that the PDA does not prevent the attachment of foulants onto the membrane surface. In industry, the membranes would be expected to retain high flux for a period of months rather than days; thus it is important that the membranes exhibit stable

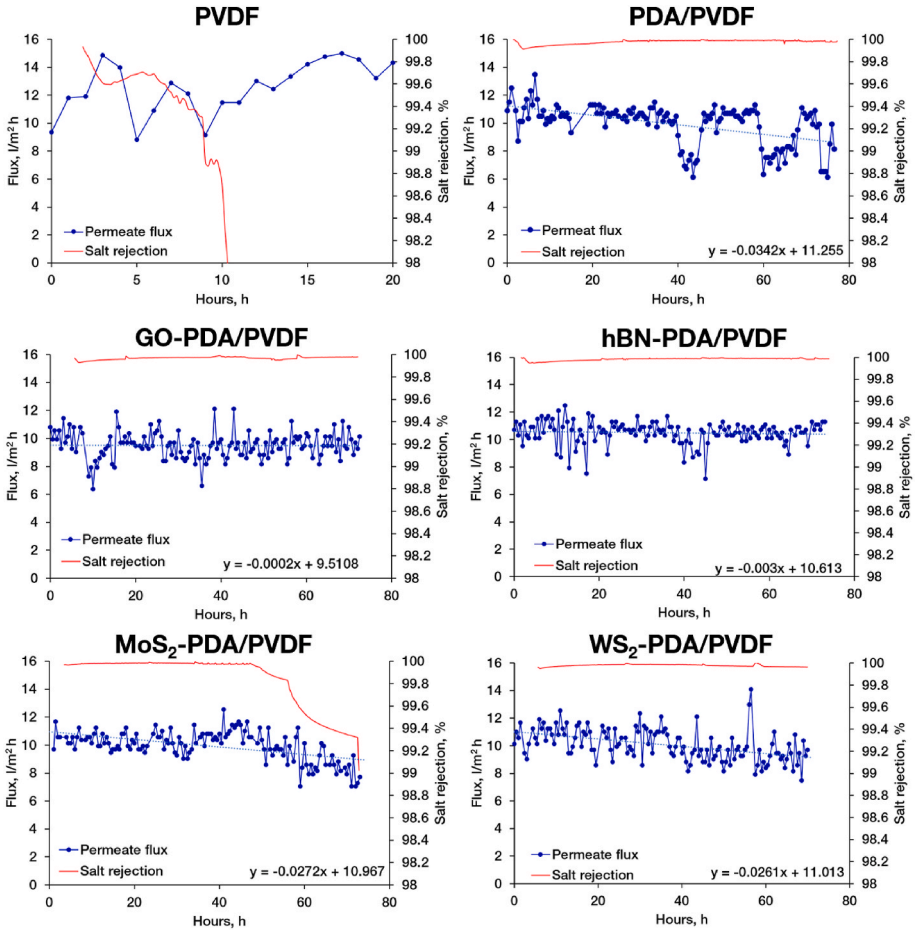

Fig. 9. Fouling performance of the following membranes over the experimental time of 72 h: commercial PVDF (experimental time of 20 h due to membrane failure); PDA-PDA control; GO-PD/PVDF; hBN-PDA/PVDF; MoS_2-PDA/PVDF and WS_2-PDA/PVDF. Feed solution: 35 g/L NaCl, 150 ppm humic acid and 200 ppm paraffin oil. Acronyms: polyvinylidene fluoride (PVDF), polydopamine (PDA), graphene oxide (GO), hexagonal boron nitride (hBN), molybdenum disulphide (MoS_2) and tungsten disulphide (WS_2).

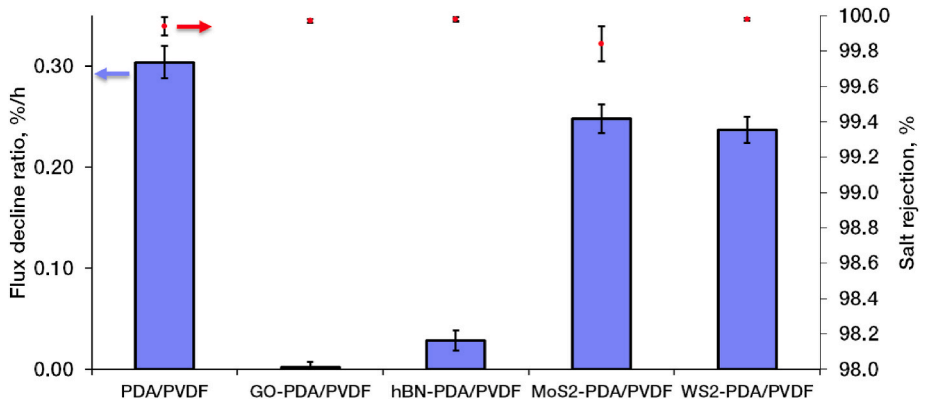

Fig. 10. Average salt rejection (%, represented as dots in red) and flux decline ratio (%/h, represented as bars in blue) for the membranes with a feed solution of 35 g/L NaCl, 150 ppm humic acid and 200 ppm of paraffin oil over the 72-h experiment. The temperature of the feed and cooling water was 75 °C and 20 °C, respectively. The error bars consider the standard deviation of the results; at least three membranes were tested per membrane type. Acronyms: polyvinylidene fluoride (PVDF), polydopamine (PDA), graphene oxide (GO), hexagonal boron nitride (hBN), molybdenum disulphide (MoS_2) and tungsten disulphide (WS_2). (For interpretation of the references to colour in this figure legend, the reader is referred to the Web version of this article.)

fouling resistance for the duration of the experiment. The other tested PDA/PVDF membranes can be found in Fig. S8. The best results were achieved with the GO-PDA/PVDF membrane, which had the highest rejection (99.98 ± 0.01 %) and lowest FDR (0.0021 ± 0.005 %/h). Over the 72 h experiment the flux for the PDA/PVDF membrane dropped by 22 %, whereas the GO-PDA/PVDF membrane had a negligible flux reduction of 0.14 % in the same time period; this shows a significant resistance to fouling. The final permeate fluxes for the PDA/PVDF and GO-PDA/PVDF membranes were 8.8 L/m^2 h and 9.5 L/m^2 h, respectively.

3.4. Membrane pore-wetting performance

All of the 2D-functionalised membranes were then tested for feed solutions containing 150 ppm Triton X-100. Pore wetting can be induced by the presence of low surface tension liquids that are miscible with water, such as alcohols and amphiphilic molecules (e.g. surfactants) [50]. Fig. 11a (left-hand side) shows that the pristine commercial membrane without the coating begins to fail 40 min after the addition of the surfactant, which is shown by the sharp decrease in salt rejection. The graphs with the raw conductivity data can be found in Fig. S9. A similar trend can be seen in Fig. S10 for the PDA/PVDF membrane, which began to fail after 45 min. As the membrane becomes fully wetted, the feedwater begins to fully penetrate the membrane pores and consequently the flux increases. The GO-PDA/PVDF membrane in Fig. 11b (right-hand side) shows that the addition of the surfactant initially reduces the salt rejection by a minor amount (<0.1 %), before the system recovers and the rejection is stable over the course of the experiment. The flux reduces across the length of the experiment, which suggests the adsorption of the surfactant onto the membrane surface. As the PVDF membranes failed after a shorter period (in comparison to the fouling experiments), the total experimental time was reduced from 72 h to 40 h. Also, the GO-PDA/PVDF membrane was the only membrane type that showed pore-wetting resistance for the entire experimental time (see Figs. S11–S13 in the SI). This could be due to more uniform and thicker layers of GO deposited as compared to the other considered 2D materials, which led to lower surface roughness and lower contact angle (Table 1).

3.5. Comparison with literature

Table 2 compares the MD water treatment performance of the membranes produced in this work with those reported in the literature for GO. No MD fouling studies could be found for MoS_2 and hBN, and no MD studies for WS_2 membranes could be found at all. However, a preliminary comparison was attempted by evaluating the permeate flux and salt rejection in the available studies. Mao et al. [83] developed GO-SiO_2 coated polyacrylonitrile membranes for the separation of 3.5 wt% NaCl solutions with 0.4 mM sodium dodecyl sulfate (SDS). The fouling results showed a decrease in the flux from approximately 14 to 8 L/m^2 h over 72 h, which gives a FDR ratio of 0.8 %/h, 12 times greater than the FDR of the GO membranes in this study.

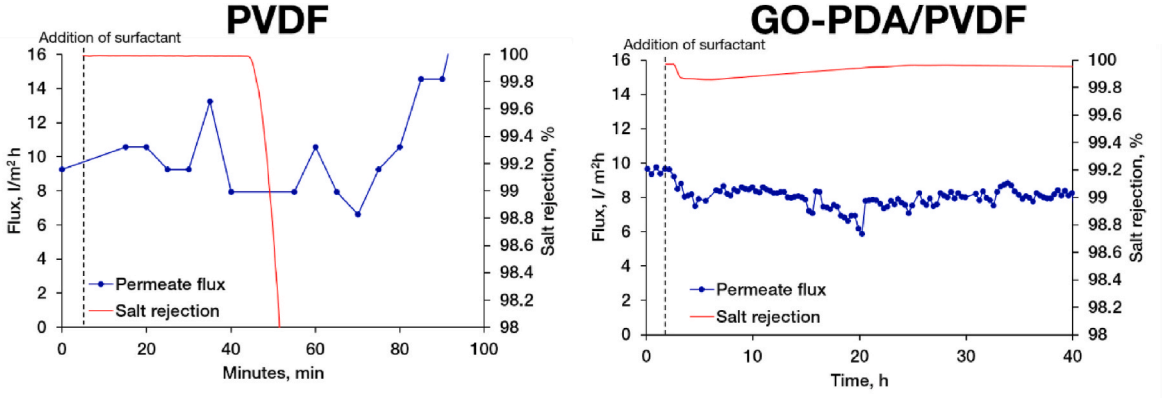

Fig. 11. Pore-wetting performance of the commercial PVDF (left; experimental time 100 min as membrane failed) and GO-PDA/PVDF membranes (right; experimental time over 40 h). Feed solution: 35 g/L NaCl and 150 ppm Triton X-100.

Table 2
A summary of the investigations using 2D materials (GO, hBN, MoS_2 and WS_2) within membrane distillation.

Membrane support	2D material	Membrane type and synthesis	Operating conditions	Performance	Role of 2D material	Ref.
PVDF	GO	Laminate membrane	Configuration: AGMD Feed solution: 35 g/L NaCl Feed temp: 75 °C Coolant temp: 20 °C Feed flow rate: 1290 mL/min Experimental time: 90 h	GO membrane increased pore wetting resistance to over 90 h compared with 20 min for pristine commercial PVDF	The laminate GO membrane has small pores which increase the LEP and lead to pore-wetting resistance	[50]
PVDF	GO functionalised with APTS	MMM Phase inversion	Configuration: AGMD Feed solution: 35 g/L NaCl Feed temp: 85 °C Coolant temp: 20 °C Feed flow rate: 380 mL/min Experimental time: 2 h	52–86 % increase in flux compared to the synthesised PVDF membrane. No fouling tests were carried out.	GO increases the speed of demixing during phase inversion. This increases the porosity and therefore the permeate flux.	[12]
PTFE and PVDF	GO	MMM PVDF/GO composite cast onto PTFE support	Configuration: DCMD Feed solution: 10 g/L NaCl Feed temp: 80 °C Coolant temp: 18 °C Feed flow rate: 200 mL/min Experimental time: 60 days	15 % increase in flux compared to the unmodified PTFE membrane. No fouling tests were carried out.	Hydrophilic GO increased condensation and vapour removal rate, which increased the driving force	[86]
PTFE	GO	MMM	Configuration: DCMD Feed solution: 3.5–34 g/L NaCl Feed temp: 80 °C Coolant temp: 20 °C Feed flow rate: 212 mL/min Experimental time: 90 days	35 % increase in flux compared to the unmodified PTFE membrane. No fouling tests were carried out.	Increase the nanocapillary effect and reduced temperature polarisation. Polar groups	[87]
PTFE	Gr	Few-layer CVD graphene wet transferred onto commercial PTFE	Configuration: DCMD Feed solution: 70 g/L NaCl, 1 mM mineral oil,1 mM SDS Feed temp: 60 °C Coolant temp: 20 °C Feed flow rate: 30 mL/min Experimental time: 48/72 h	High rejection (99.9 %) Anti-wetting properties (rejection >99.9 % over 48 h compared with 87 %) Antifouling properties (flux decline 54 to 49 L/m^2 h compared to 62 to 38 L/m^2 h).	Charge neutrality helps with antifouling. Weak physisorption of SDS on graphene. Poor thermal conductivity in the z-direction, leading to reduced heat loss.	[88]
PTFE	rGO	Laminate	Configuration: DCMD Feed solution: 35 g/L NaCl, 0.8 mM SDS Feed temp: 60–80 °C Coolant temp: 20 °C Feed flow rate: unknown Experimental time: 66 h	Wetting resistance against 0.8 mM SDS for 66 h. High flux (149 L/m^2 h) at high temperature differences	rGO suppressed temperature polarisation which increased the flux. Anti-wetting properties were due to low water adsorption of rGO	[89]
PAN	GO functionalised with SiO_2 and long alkyl chains	MMM	Configuration: VMD Feed solution: 35 g/L NaCl, 0.4 mM SDS, 30 mg/L humic acid Feed temp: 60 °C Coolant temp: 20 °C Feed flow rate: unknown Experimental time: 170 h	Flux reduced from ~14 to 7 L/m^2 h over 170 h with SDS feed. Stable salt rejection for the entire experiment	Increased hydrophobicity and roughness, leading to enhanced antifouling properties	[83]
PVDF	MoS_2	Coating	Configuration: DCMD Feed solution: 58 g/L NaCl, 2 w/v% ethylene glycol, 0.1 Mm SDS Feed temp: 60 °C Coolant temp: 20 °C Feed flow rate: 200	Water flux 27 L/m^2 h, but this decreased to 21 L/m^2 h over 8 h	MoS_2-made membrane omniphobic with low surface electrical resistance	[13]

(*continued on next page*)

Table 2 (*continued*)

Membrane support	2D material	Membrane type and synthesis	Operating conditions	Performance	Role of 2D material	Ref.
			mL/min Experimental time: 8 h			
Ceramic β-sialon	hBN	Coating	Configuration: SGMD Feed solution: 40 g/L NaCl Feed temp: 80 °C Coolant temp: unknown Feed flow rate: 1000 mL/min Experimental time: 200 h	Reject rate of 99.9 % and stable flux of 5–6 L/m^2 h over 200 h. No comparison with unmodified membrane and no fouling tests were carried out.	hBN increased the membrane hydrophobicity (145°)	[29]
PVDF/ polyethylene glycol	hBN	MMM	Configuration: DCMD and MDC Feed solution: K_2SO_4 and KNO_3 Feed temp: 80 °C Coolant temp: 20 °C Feed flow rate: 700 mL/min Experimental time: 100 h	Higher recovery of salts (for membrane crystallisation) and ~60 % higher flux[a] when compared to unmodified membrane	Polar B–N bonds aided the separation of water through the nanochannels. hBN increased the membrane porosity	[30]
PVDF	hBN	MMM	Configuration: AGMD Feed solution: 35 g/L NaCl Feed temp: 80 °C Coolant temp: 20 °C Feed flow rate: 250 mL/min Experimental time: 60 h	43 % increase in flux compared to PVDF. No fouling tests were carried out.	hBN increased the membrane porosity by acting as crystallisation nuclei during the demixing stage of membrane manufacturing	[31]
PVDF	GO-PDA	Pyrolyser for surface functionalisation, and immobilised using PDA	Configuration: AGMD Feed solution: 35 g/L NaCl, 150 ppm humic acid, 200 ppm paraffin oil Feed temp: 75 °C Coolant temp: 20 °C Feed flow rate: 1000 mL/min Experimental time: 72 h	Stable operation over 72 h compared to ~10 h for control. Initial flux: 9.51 L/m^2 h Final flux: 9.50 L/m^2 h FDR of 0.0021 ± 0.005 %/h 7 % increase in permeate flux	Increased hydrophilicity and reduced surface roughness which reduced fouling attachment	This work
PVDF	hBN-PDA	Pyrolyser for surface functionalisation and immobilised using PDA	Configuration: AGMD Feed solution: 35 g/L NaCl, 150 ppm humic acid, 200 ppm paraffin oil Feed temp: 75 °C Coolant temp: 20 °C Feed flow rate: 1000 mL/min Experimental time: 72 h	Stable operation over 72 h (compared to ~10 h for control) Unstable for Triton X-100 feed Initial flux: 10.6 L/m^2 h Final flux: 10.4 L/m^2 h FDR of 0.0274 ± 0.01 %/h 12 % increase in permeate flux	Increased hydrophilicity and reduced surface roughness which reduced fouling attachment	This work
PVDF	MoS_2-PDA	Pyrolyser for surface functionalisation and immobilised using PDA	Configuration: AGMD Feed solution: 35 g/L NaCl, 150 ppm humic acid, 200 ppm paraffin oil Feed temp: 75 °C Coolant temp: 20 °C Feed flow rate: 1000 mL/min Experimental time: 72 h	Stable operation over 72 h (compared to ~10 h for control) Unstable for Triton X-100 feed Initial flux: 11.0 L/m^2 h Final flux: 9.01 L/m^2 h FDR of 0.25 ± 0.014 %/h 10 % increase in permeate flux		This work
PVDF	WS_2-PDA	Pyrolyser for surface functionalisation and immobilised using PDA	Configuration: AGMD Feed solution: 35 g/L NaCl, 150 ppm humic acid, 200 ppm paraffin oil Feed temp: 75 °C Coolant temp: 20 °C Feed flow rate: 1000 mL/min Experimental time: 72 h	Stable operation over 72 h (compared to ~10 h for control) Unstable for Triton X-100 feed Initial flux: 11.0 L/m^2 h Final flux: 9.12 L/m^2 h FDR of 0.24 ± 0.013 %/h 12 % increase in permeate flux		This work

Acronyms: Air gap membrnae distillation (AGMD); 3-(aminopropyl)triethoxysilane (APTS); direct contact membrane distillation (DCMD); flux decline ratio (FDR); graphene oxide (GO); hexagonal boron nitride (hBN); membrane distillation crystallisation (MDC); mixed matrix membrane (MMM); molybdenum disulphide (MoS_2); polyacrylonitrile (PAN); PTFE: Polytetrafluoroethylene; polyvinylidene fluoride (PVDF); polydopamine (PDA); sweeping gas membrane distillation (SGMD); vacuum membrane distillation (VMD); tungsten disulphide (WS_2).

[a] Value calculated from available data.

In many fouling studies, the development of an antifouling layer usually comes with a decrease in the permeate flux. For example, Li et al. [84] investigated Janus membranes for the desalination of saline oily wastewater. The omniphobic quartz membrane (which was developed for its antifouling and pore-wetting resistance) had an initial flux of 19 L/m^2 h, whereas the original quartz fibre membrane had a flux of 28.6 L/m^2 h. This 34 % reduction in the permeate flux is significant and it can also be seen in other MD fouling work. Mansour et al. [85] developed graphene nanoplatelet (GP) coated membranes for brine treatment via DCMD. The best GP coating (0.16 wt%) had a low flux reduction (15-14 L/m^2 h over 10 h) which indicates antifouling properties. However, even the initial permeate flux was still lower than the final flux of the pristine commercial membrane, which reduced from 30 to 22 L/m^2 h over the same time period. The membranes studied in this investigation reduced the FDR but did not reduce the flux of the membranes when compared to the controls. This is likely due to the capillary force provided by the 2D flakes, which increases the vapour pressure difference between the feed and permeate side. The PDA is an insulating material and could also reduce the heat loss, which increases flux when compared to the PVDF control.

The GO-PDA/PVDF membranes synthesised in this study achieved a similar permeate flux when compared to membranes in our previous study, in which GO was deposited via vacuum filtration [50]. Also, in the current study, the immobilisation of the GO could have improved as a result of the spray coating method, whereby the amount of GO in water was 3.69 mg/m^2 compared with 19.6 mg/m^2. However, this is assuming that the quantity of deposited GO is equivalent for both methods.

Overall, the GO-PDA/PVDF membrane should be selected to treat wastewater containing organic and oil foulants as it reduced the FDR from 22 % to 0.14 % over the 72 h experiment. However, this membrane also resulted in the lowest tensile strength. For MD applications, this may be of little importance as the physical strain that the membranes are under is low (when operated at ambient pressure). However, for high-pressure applications, such as reverse osmosis and nanofiltration, the hBN and WS_2 coating may be more suitable to provide fouling resistance without affecting mechanical durability.

4. Conclusions

In this study, a new scalable method for depositing 2D flakes onto polymer substrates was described and demonstrated for graphene oxide (GO), hexagonal boron nitride (hBN), molybdenum disulphide (MoS_2) and tungsten disulphide (WS_2). Characterisation of the GO membrane showed that a thin layer of 2D material was deposited using this method. The fouling results revealed that GO and hBN had the highest fouling resistance, with negligible flux decline ratios over 72 h for a feed with 150 ppm humic acid and 200 ppm paraffin oil. The GO membranes were the only type that were resistant to both fouling and pore wetting, which was demonstrated by the stable flux during MD operation with 150 ppm surfactant Triton X-100. The hBN membranes performed better under mechanical testing, with significantly higher tensile strength (7 MPa) and strain (68.8 %) than the GO membranes (5 MPa and 41.3 %, respectively). However, mechanical properties and stability of GO membranes indicate no concerns for their scalability. In fact, the proposed coating method outlined in this work is scalable, but future work should demonstrate this through the manufacture of pilot-sized membranes and testing with more realistic wastewater samples. This work is currently being carried out by the authors as a follow-up to this research. Looking further ahead, as GO, MoS_2 and WS_2 are excellent conductors of heat, future work could also consider exploring these materials as thin-films for localised Joule-heating, as well as investigating a combination of two or more of these 2D materials within one membrane.

CRediT authorship contribution statement

Clara Skuse: Writing – original draft, Investigation, Formal analysis, Conceptualization. **Monica Alberto:** Investigation. **José Miguel Luque-Alled:** Investigation. **Vicente Orts Mercadillo:** Resources, Investigation. **Edidiong Asuquo:** Resources, Investigation. **Alejandro Gallego-Schmid:** Writing – review & editing, Supervision. **Adisa Azapagic:** Writing – review & editing, Supervision. **Patricia Gorgojo:** Writing – review & editing, Supervision, Project administration, Funding acquisition, Conceptualization.

Declaration of competing interest

The authors declare that they have no known competing financial interests or personal relationships that could have appeared to influence the work reported in this paper.

Data availability

Data will be made available on request.

Acknowledgements

The authors are grateful to the EPSRC for funding under grant number EP/S032258/1. Clara Skuse would like to acknowledge the EPSRC for funding this work through the NOWNANO CDT. Patricia Gorgojo is grateful for her Fellowship with reference RYC2019-027060-I funded by MCIN/AEI/10.13039/501100011033 and European Union NextGenerationEU/PRTR. The authors would also like to thank Dr Liam Britnell for his expertise, Dr Jason Hui for his preliminary material supply, Dr Nigel Hodson for his technical support with AFM and Andy Skuse for his proofreading help.

Appendix A. Supplementary data

Supplementary data to this article can be found online at https://doi.org/10.1016/j.memsci.2024.123162.

References

[1] S.P. Nunes, P.Z. Culfaz-Emecen, G.Z. Ramon, T. Visser, G.H. Koops, W. Jin, M. Ulbricht, Thinking the future of membranes: perspectives for advanced and new membrane materials and manufacturing processes, J. Membr. Sci. 598 (2020) 117761, https://doi.org/10.1016/j.memsci.2019.117761.

[2] A. Alkhatib, M.A. Ayari, A.H. Hawari, Fouling mitigation strategies for different foulants in membrane distillation, Chemical Engineering and Processing - Process Intensification 167 (2021) 108517, https://doi.org/10.1016/j.cep.2021.108517.

[3] S. Kalla, Use of membrane distillation for oily wastewater treatment – a review, J. Environ. Chem. Eng. 9 (1) (2021) 104641, https://doi.org/10.1016/j.jece.2020.104641.

[4] G. Yang, J. Zhang, M. Peng, E. Du, Y. Wang, G. Shan, L. Ling, H. Ding, S. Gray, Z. Xie, A mini review on antiwetting studies in membrane distillation for textile wastewater treatment, Processes 9 (2) (2021) 243.

[5] A.A. Kiss, O.M. Kattan Readi, An industrial perspective on membrane distillation processes, J. Chem. Technol. Biotechnol. 93 (8) (2018) 2047–2055, https://doi.org/10.1002/jctb.5674.

[6] M. Gryta, Resistance of polypropylene membrane to oil fouling during membrane distillation, Membranes 11 (8) (2021) 552.

[7] N.G.P. Chew, S. Zhao, R. Wang, Recent advances in membrane development for treating surfactant- and oil-containing feed streams via membrane distillation, Adv. Colloid Interface Sci. 273 (2019) 102022, https://doi.org/10.1016/j.cis.2019.102022.

[8] C. Skuse, A. Gallego-Schmid, A. Azapagic, P. Gorgojo, Can emerging membrane-based desalination technologies replace reverse osmosis? Desalination 500 (2021) 114844 https://doi.org/10.1016/j.desal.2020.114844.
[9] S. Zare, A. Kargari, 4 - Membrane properties in membrane distillation, in: V.G. Gude (Ed.), Emerging Technologies for Sustainable Desalination Handbook, Butterworth-Heinemann2018, pp. 107-156. https://doi.org/10.1016/B978-0-12-815818-0.00004-7.
[10] L. Han, T. Xiao, Y.Z. Tan, A.G. Fane, J.W. Chew, Contaminant rejection in the presence of humic acid by membrane distillation for surface water treatment, J. Membr. Sci. 541 (2017) 291–299, https://doi.org/10.1016/j.memsci.2017.07.013.
[11] M. Frappa, A.E. Del Rio Castillo, F. Macedonio, A. Politano, E. Drioli, F. Bonaccorso, V. Pellegrini, A. Gugliuzza, A few-layer graphene for advanced composite PVDF membranes dedicated to water desalination: a comparative study, Nanoscale Adv. 2 (10) (2020) 4728–4739, https://doi.org/10.1039/D0NA00403K.
[12] S. Leaper, A. Abdel-Karim, B. Faki, J.M. Luque-Alled, M. Alberto, A. Vijayaraghavan, S.M. Holmes, G. Szekely, M.I. Badawy, N. Shokri, P. Gorgojo, Flux-enhanced PVDF mixed matrix membranes incorporating APTS-functionalized graphene oxide for membrane distillation, J. Membr. Sci. 554 (2018) 309–323, https://doi.org/10.1016/j.memsci.2018.03.013.
[13] E.L. Koh, Yong Taek 2D nanosheet MoS 2-G-PVDF nanocomposite omniphobic membrane for the removal of low-surface-tension-liquid in membrane distillation, SSRN Electron. J. (2022). Available at SSRN: https://ssrn.com/abstract=4036636.
[14] C. Lee, X. Wei, J.W. Kysar, J. Hone, Measurement of the elastic properties and intrinsic strength of monolayer graphene, Science 321 (5887) (2008) 385–388, https://doi.org/10.1126/science.1157996.
[15] D.G. Papageorgiou, I.A. Kinloch, R.J. Young, Mechanical properties of graphene and graphene-based nanocomposites, Prog. Mater. Sci. 90 (2017) 75–127, https://doi.org/10.1016/j.pmatsci.2017.07.004.
[16] K.S. Novoselov, A.K. Geim, S.V. Morozov, D. Jiang, Y. Zhang, S.V. Dubonos, I. V. Grigorieva, A.A. Firsov, Electric field effect in atomically thin carbon films, Science 306 (5696) (2004) 666–669, https://doi.org/10.1126/science.1102896.
[17] A.A. Balandin, S. Ghosh, W. Bao, I. Calizo, D. Teweldebrhan, F. Miao, C.N. Lau, Superior thermal conductivity of single-layer graphene, Nano Lett. 8 (3) (2008) 902–907, https://doi.org/10.1021/nl0731872.
[18] G.-h. Yang, D.-d. Bao, H. Liu, D.-q. Zhang, N. Wang, H.-t. Li, Functionalization of graphene and applications of the derivatives, J. Inorg. Organomet. Polym. Mater. 27 (5) (2017) 1129–1141, https://doi.org/10.1007/s10904-017-0597-6.
[19] T. Kuilla, S. Bhadra, D. Yao, N.H. Kim, S. Bose, J.H. Lee, Recent advances in graphene based polymer composites, Prog. Polym. Sci. 35 (11) (2010) 1350–1375, https://doi.org/10.1016/j.progpolymsci.2010.07.005.
[20] R.R. Nair, H.A. Wu, P.N. Jayaram, I.V. Grigorieva, A.K. Geim, Unimpeded permeation of water through helium-leak–tight graphene-based membranes, Science 335 (6067) (2012) 442–444, https://doi.org/10.1126/science.1211694.
[21] R.K. Joshi, P. Carbone, F.C. Wang, V.G. Kravets, Y. Su, I.V. Grigorieva, H.A. Wu, A. K. Geim, R.R. Nair, Precise and ultrafast molecular sieving through graphene oxide membranes, Science 343 (6172) (2014) 752–754, https://doi.org/10.1126/science.1245711.
[22] J. Deng, Y. You, H. Bustamante, V. Sahajwalla, R.K. Joshi, Mechanism of water transport in graphene oxide laminates, Chem. Sci. 8 (3) (2017) 1701–1704, https://doi.org/10.1039/C6SC03909J.
[23] G. Liu, W. Jin, N. Xu, Graphene-based membranes, Chem. Soc. Rev. 44 (15) (2015) 5016–5030, https://doi.org/10.1039/C4CS00423J.
[24] P. Sun, K. Wang, H. Zhu, Recent developments in graphene-based membranes: structure, mass-transport mechanism and potential applications, Adv. Mater. 28 (12) (2016) 2287–2310, https://doi.org/10.1002/adma.201502595.
[25] M.H. Köhler, J.P.K. Abal, G.V. Soares, M.C. Barbosa, Molybdenum disulfide and tungsten disulfide as novel two-dimensional nanomaterials in separation science, in: R. Das (Ed.), Two-Dimensional (2D) Nanomaterials in Separation Science, Springer International Publishing, Cham, 2021, pp. 193–217, https://doi.org/10.1007/978-3-030-72457-3_8.
[26] Y. Liu, Y. Zhao, X. Zhang, X. Huang, W. Liao, Y. Zhao, MoS2-based membranes in water treatment and purification, Chem. Eng. J. 422 (2021) 130082, https://doi.org/10.1016/j.cej.2021.130082.
[27] P.O. Oviroh, T.-C. Jen, J. Ren, L.M. Mohlala, R. Warmbier, S. Karimzadeh, Nanoporous MoS2 membrane for water desalination: a molecular dynamics study, Langmuir 37 (23) (2021) 7127–7137, https://doi.org/10.1021/acs.langmuir.1c00708.
[28] L. Liu, Y. Liu, Y. Qi, M. Song, L. Jiang, G. Fu, J. Li, Hexagonal boron nitride with nanoslits as a membrane for water desalination: a molecular dynamics investigation, Separ. Purif. Technol. 251 (2020) 117409, https://doi.org/10.1016/j.seppur.2020.117409.
[29] R. Qian, B. Dong, S. Hao, F. Wang, L. Wang, Z. Min, L. Hao, X. Xu, S. Agathopoulos, Robust all-inorganic hydrophobic BN nanosheets coated β-sialon membrane for membrane distillation, J. Eur. Ceram. Soc. 42 (6) (2022) 2672–2677, https://doi.org/10.1016/j.jeurceramsoc.2022.02.002.
[30] A. Srivastava, Z.V.P. Murthy, Investigating the effect of PEG200 and two-dimensional h-BN on PVDF membrane performance for membrane distillation–crystallization, Mater. Today Chem. 22 (2021) 100545, https://doi.org/10.1016/j.mtchem.2021.100545.
[31] J. Zahirifar, A. Hadi, J. Karimi-Sabet, A. Dastbaz, Influence of hexagonal boron nitride nanosheets as the additives on the characteristics and performance of PVDF for air gap membrane distillation, Desalination 460 (2019) 81–91, https://doi.org/10.1016/j.desal.2019.03.004.
[32] D. Lee, Y.C. Woo, K.H. Park, S. Phuntsho, L.D. Tijing, M. Yao, W.-G. Shim, H. K. Shon, Polyvinylidene fluoride phase design by two-dimensional boron nitride enables enhanced performance and stability for seawater desalination, J. Membr. Sci. 598 (2020) 117669, https://doi.org/10.1016/j.memsci.2019.117669.
[33] S. Leaper, A. Abdel-Karim, P. Gorgojo, The use of carbon nanomaterials in membrane distillation membranes: a review, Front. Chem. Sci. Eng. 15 (4) (2021) 755–774, https://doi.org/10.1007/s11705-020-1993-y.
[34] S. Seraj, T. Mohammadi, M.A. Tofighy, Graphene-based membranes for membrane distillation applications: a review, J. Environ. Chem. Eng. 10 (3) (2022) 107974, https://doi.org/10.1016/j.jece.2022.107974.
[35] W. Hirunpinyopas, E. Prestat, S.D. Worrall, S.J. Haigh, R.A.W. Dryfe, M.A. Bissett, Desalination and nanofiltration through functionalized laminar MoS2 membranes, ACS Nano 11 (11) (2017) 11082–11090, https://doi.org/10.1021/acsnano.7b05124.
[36] Y. Su, D. Liu, G. Yang, Q. Han, Y. Qian, Y. Liu, L. Wang, J.M. Razal, W. Lei, Transition metal dichalcogenide (TMD) membranes with ultrasmall nanosheets for ultrafast molecule separation, ACS Appl. Mater. Interfaces 12 (40) (2020) 45453–45459, https://doi.org/10.1021/acsami.0c10653.
[37] H. Zhang, Y. Zheng, S. Yu, W. Chen, J. Yang, A review of advancing two-dimensional material membranes for ultrafast and highly selective liquid separation, Nanomaterials 12 (12) (2022) 2103.
[38] F. Arshad, C. Aubry, F. Ravaux, L. Zou, 2D MoS2 nanoplatelets for fouling resistant membrane surface, J. Colloid Interface Sci. 590 (2021) 415–423, https://doi.org/10.1016/j.jcis.2021.01.085.
[39] S. Vetrivel, M. Sri Abirami Saraswathi, D. Rana, K. Divya, A. Nagendran, Cellulose acetate composite membranes tailored with exfoliated tungsten disulfide nanosheets: permeation characteristics and antifouling ability, Int. J. Biol. Macromol. 115 (2018) 540–546, https://doi.org/10.1016/j.ijbiomac.2018.04.091.
[40] J. Lin, R. Zhang, W. Ye, N. Jullok, A. Sotto, B. Van der Bruggen, Nano-WS2 embedded PES membrane with improved fouling and permselectivity, J. Colloid Interface Sci. 396 (2013) 120–128, https://doi.org/10.1016/j.jcis.2013.01.028.
[41] D.L. Keshebo, C.-C. Hu, W.-S. Hung, C.-F. Wang, H.-C. Tsai, K.-R. Lee, J.-Y. Lai, Simultaneous exfoliation and functionalization of hexagonal boron nitride in the aqueous phase for the synthesis of high-performance wastewater treatment membrane, J. Clean. Prod. 314 (2021) 128083, https://doi.org/10.1016/j.jclepro.2021.128083.
[42] M. Rostami, D. Jahani Sabet, V. Vatanpour, Fabrication of antifouling two-dimensional MoS2 layered PVDF membrane: experimental and density functional theory calculation, Separ. Purif. Technol. 303 (2022) 122226, https://doi.org/10.1016/j.seppur.2022.122226.
[43] R.S.-N. Moradi, Mojtaba, N.M. Poukhalili, Masoud, H. Niknafs, PVDF/h-BN hybrid membranes and their application in desalination through AGMD, Membrane Water Treatment 9 (2018), https://doi.org/10.12989/mwt.2018.9.4.221.
[44] Z. Yan, X. Chen, S. Bao, H. Chang, H. Liu, G. Fan, Q. Wang, X. Fu, F. Qu, H. Liang, Integration of in situ Fenton-like self-cleaning and photothermal membrane distillation for wastewater treatment via Co-MoS2/CNT catalytic membrane, Separ. Purif. Technol. 303 (2022) 122207, 0.1016/j.seppur.2022.122207.
[45] M. Zhang, Y. Mao, G. Liu, G. Liu, Y. Fan, W. Jin, Molecular bridges stabilize graphene oxide membranes in water, Angew. Chem. Int. Ed. 59 (4) (2020) 1689–1695, https://doi.org/10.1002/anie.201913010.
[46] P. Cheng, L.-L. Ye, S.-C. Wu, Y. Chen, X. Yan, X.-J. Guo, W.-Z. Lang, Amorphous TiO2 bridges stabilized WS2 membranes with excellent filtration stability and photocatalysis-driving self-cleaning ability, ACS Appl. Mater. Interfaces 13 (48) (2021) 58076–58084, https://doi.org/10.1021/acsami.1c14967.
[47] H. Tian, X. Wu, K. Zhang, Polydopamine-Assisted two-dimensional molybdenum disulfide (MoS2)-modified PES tight ultrafiltration mixed-matrix membranes: enhanced dye separation performance, Membranes 11 (2) (2021) 96.
[48] Q. Feng, Y. Zhan, W. Yang, A. Sun, H. Dong, Y.-H. Chiao, Y. Liu, X. Chen, Y. Chen, Bi-functional super-hydrophilic/underwater super-oleophobic 2D lamellar Ti3C2Tx MXene/poly (arylene ether nitrile) fibrous composite membrane for the fast purification of emulsified oil and photodegradation of hazardous organics, J. Colloid Interface Sci. 612 (2022) 156–170, https://doi.org/10.1016/j.jcis.2021.12.160.
[49] R.P. Pandey, P. Kallem, H.M. Hegab, P.A. Rasheed, F. Banat, S.W. Hasan, Cross-linked laminar graphene oxide membranes for wastewater treatment and desalination: a review, J. Environ. Manag. 317 (2022) 115367, https://doi.org/10.1016/j.jenvman.2022.115367.
[50] M. Alberto, C. Skuse, M. Tamaddondar, P. Gorgojo, Immobilized graphene oxide-based membranes for improved pore wetting resistance in membrane distillation, Desalination 537 (2022) 115898, https://doi.org/10.1016/j.desal.2022.115898.
[51] W.-S. Hung, T.-J. Lin, Y.-H. Chiao, A. Sengupta, Y.-C. Hsiao, S.R. Wickramasinghe, C.-C. Hu, K.-R. Lee, J.-Y. Lai, Graphene-induced tuning of the d-spacing of graphene oxide composite nanofiltration membranes for frictionless capillary action-induced enhancement of water permeability, J. Mater. Chem. A 6 (40) (2018) 19445–19454, https://doi.org/10.1039/C8TA08155G.
[52] R. Das, P. Solís-Fernández, D. Breite, A. Prager, A. Lotnyk, A. Schulze, H. Ago, High flux and adsorption based non-functionalized hexagonal boron nitride lamellar membrane for ultrafast water purification, Chem. Eng. J. 420 (2021) 127721, https://doi.org/10.1016/j.cej.2020.127721.
[53] L. Sun, Y. Ying, H. Huang, Z. Song, Y. Mao, Z. Xu, X. Peng, Ultrafast molecule separation through layered WS2 nanosheet membranes, ACS Nano 8 (6) (2014) 6304–6311, https://doi.org/10.1021/nn501786m.
[54] H.M. Hegab, L. Zou, Graphene oxide-assisted membranes: fabrication and potential applications in desalination and water purification, J. Membr. Sci. 484 (2015) 95–106, https://doi.org/10.1016/j.memsci.2015.03.011.
[55] L. Chen, J.-H. Moon, X. Ma, L. Zhang, Q. Chen, L. Chen, R. Peng, P. Si, J. Feng, Y. Li, J. Lou, L. Ci, High performance graphene oxide nanofiltration membrane

prepared by electrospraying for wastewater purification, Carbon 130 (2018) 487–494, https://doi.org/10.1016/j.carbon.2018.01.062.
[56] M. Nunnenkamp, K.J.H. van den Nieuwenhuijzen, J.E. ten Elshof, Multilayer films of exfoliated 2D oxide nanosheets by electrospray deposition, Sci. Rep. 12 (1) (2022) 8673, https://doi.org/10.1038/s41598-022-12768-3.
[57] A. Jaworek, A.T. Sobczyk, Electrospraying route to nanotechnology: an overview, J. Electrost. 66 (3) (2008) 197–219, https://doi.org/10.1016/j.elstat.2007.10.001.
[58] J. Leng, Z. Wang, J. Wang, H.-H. Wu, G. Yan, X. Li, H. Guo, Y. Liu, Q. Zhang, Z. Guo, Advances in nanostructures fabricated via spray pyrolysis and their applications in energy storage and conversion, Chem. Soc. Rev. 48 (11) (2019) 3015–3072, https://doi.org/10.1039/C8CS00904J.
[59] M. Lengyel, D. Elhassid, G. Atlas, W.T. Moller, R.L. Axelbaum, Development of a scalable spray pyrolysis process for the production of non-hollow battery materials, J. Power Sources 266 (2014) 175–178, https://doi.org/10.1016/j.jpowsour.2014.04.143.
[60] P. Nie, G. Xu, J. Jiang, H. Dou, Y. Wu, Y. Zhang, J. Wang, M. Shi, R. Fu, X. Zhang, Aerosol-spray pyrolysis toward preparation of nanostructured materials for batteries and supercapacitors, Small Methods 2 (2) (2018) 1700272, https://doi.org/10.1002/smtd.201700272.
[61] A. Abdel-Karim, S. Leaper, C. Skuse, G. Zaragoza, M. Gryta, P. Gorgojo, Membrane cleaning and pretreatments in membrane distillation – a review, Chem. Eng. J. 422 (2021) 129696, https://doi.org/10.1016/j.cej.2021.129696.
[62] F. Ricceri, M. Giagnorio, G. Farinelli, G. Blandini, M. Minella, D. Vione, A. Tiraferri, Desalination of produced water by membrane distillation: effect of the feed components and of a pre-treatment by fenton oxidation, Sci. Rep. 9 (1) (2019) 14964, https://doi.org/10.1038/s41598-019-51167-z.
[63] M. Afsari, M.J. Park, N.J. Kaleekkal, M.M. Motsa, H.K. Shon, L. Tijing, Janus distillation membrane via mussel-inspired inkjet printing modification for anti-oil fouling membrane distillation, Membranes 13 (2) (2023) 191.
[64] C. Ligorio, M. O'Brien, N.W. Hodson, A. Mironov, M. Iliut, A.F. Miller, A. Vijayaraghavan, J.A. Hoyland, A. Saiani, TGF-β3-loaded graphene oxide - self-assembling peptide hybrid hydrogels as functional 3D scaffolds for the regeneration of the nucleus pulposus, Acta Biomater. 127 (2021) 116–130, https://doi.org/10.1016/j.actbio.2021.03.077.
[65] K. Boussu, B. Van der Bruggen, A. Volodin, J. Snauwaert, C. Van Haesendonck, C. Vandecasteele, Roughness and hydrophobicity studies of nanofiltration membranes using different modes of AFM, J. Colloid Interface Sci. 286 (2) (2005) 632–638, https://doi.org/10.1016/j.jcis.2005.01.095.
[66] D. Yang, A. Velamakanni, G. Bozoklu, S. Park, M. Stoller, R.D. Piner, S. Stankovich, I. Jung, D.A. Field, C.A. Ventrice, R.S. Ruoff, Chemical analysis of graphene oxide films after heat and chemical treatments by X-ray photoelectron and Micro-Raman spectroscopy, Carbon 47 (1) (2009) 145–152, https://doi.org/10.1016/j.carbon.2008.09.045.
[67] X. Li, J. Liu, K. Ding, X. Zhao, S. Li, W. Zhou, B. Liang, Temperature dependence of Raman-active in-plane E2g phonons in layered graphene and h-BN flakes, Nanoscale Res. Lett. 13 (1) (2018) 25, https://doi.org/10.1186/s11671-018-2444-2.
[68] R. Saito, Y. Tatsumi, S. Huang, X. Ling, M.S. Dresselhaus, Raman spectroscopy of transition metal dichalcogenides, J. Phys. Condens. Matter 28 (35) (2016) 353002, https://doi.org/10.1088/0953-8984/28/35/353002.
[69] I. Sengupta, S. Chakraborty, M. Talukdar, S.K. Pal, S. Chakraborty, Thermal reduction of graphene oxide: how temperature influences purity, J. Mater. Res. 33 (23) (2018) 4113–4122, https://doi.org/10.1557/jmr.2018.338.
[70] N. Kostoglou, K. Polychronopoulou, C. Rebholz, Thermal and chemical stability of hexagonal boron nitride (h-BN) nanoplatelets, Vacuum 112 (2015) 42–45, https://doi.org/10.1016/j.vacuum.2014.11.009.
[71] N. Bandaru, R.S. Kumar, D. Sneed, O. Tschauner, J. Baker, D. Antonio, S.-N. Luo, T. Hartmann, Y. Zhao, R. Venkat, Effect of pressure and temperature on structural stability of MoS2, J. Phys. Chem. C 118 (6) (2014) 3230–3235, https://doi.org/10.1021/jp410167k.
[72] S. Pace, M. Ferrera, D. Convertino, G. Piccinini, M. Magnozzi, N. Mishra, S. Forti, F. Bisio, M. Canepa, F. Fabbri, C. Coletti, Thermal stability of monolayer WS2 in BEOL conditions, J. Phys.: Materials 4 (2) (2021) 024002, https://doi.org/10.1088/2515-7639/abd4f2.
[73] R. Xu, K. Zhang, X. Xu, M. He, F. Lu, B. Su, Superhydrophobic WS2-nanosheet-wrapped sponges for underwater detection of tiny vibration, Adv. Sci. 5 (4) (2018) 1700655, https://doi.org/10.1002/advs.201700655.
[74] Y. Zhang, F. Shen, W. Cao, Y. Wan, Hydrophilic/hydrophobic Janus membranes with a dual-function surface coating for rapid and robust membrane distillation desalination, Desalination 491 (2020) 114561, https://doi.org/10.1016/j.desal.2020.114561.
[75] L.N. Nthunya, L. Gutierrez, N. Khumalo, S. Derese, B.B. Mamba, A.R. Verliefde, S. D. Mhlanga, Superhydrophobic PVDF nanofibre membranes coated with an organic fouling resistant hydrophilic active layer for direct-contact membrane distillation, Colloids Surf. A Physicochem. Eng. Asp. 575 (2019) 363–372, https://doi.org/10.1016/j.colsurfa.2019.05.031.
[76] A. Samadi, T. Ni, E. Fontananova, G. Tang, H. Shon, S. Zhao, Engineering antiwetting hydrophobic surfaces for membrane distillation: a review, Desalination 563 (2023) 116722, https://doi.org/10.1016/j.desal.2023.116722.
[77] J.I. Paredes, S. Villar-Rodil, A. Martínez-Alonso, J.M.D. Tascón, Graphene oxide dispersions in organic solvents, Langmuir 24 (19) (2008) 10560–10564, https://doi.org/10.1021/la801744a.
[78] L. Song, L. Ci, H. Lu, P.B. Sorokin, C. Jin, J. Ni, A.G. Kvashnin, D.G. Kvashnin, J. Lou, B.I. Yakobson, P.M. Ajayan, Large scale growth and characterization of atomic hexagonal boron nitride layers, Nano Lett. 10 (8) (2010) 3209–3215, https://doi.org/10.1021/nl1022139.
[79] L. Muscuso, S. Cravanzola, F. Cesano, D. Scarano, A. Zecchina, Optical, vibrational, and structural properties of MoS2 nanoparticles obtained by exfoliation and fragmentation via ultrasound cavitation in isopropyl alcohol, J. Phys. Chem. C 119 (7) (2015) 3791–3801, https://doi.org/10.1021/jp511973k.
[80] A.K. Mishra, K.V. Lakshmi, L. Huang, Eco-friendly synthesis of metal dichalcogenides nanosheets and their environmental remediation potential driven by visible light, Sci. Rep. 5 (1) (2015) 15718, https://doi.org/10.1038/srep15718.
[81] M. Amini, A. Ramazani S A, A. Kheradmand, In-Situ polymerization of UHMWPE using Bi-supported ziegler-natta catalyst of MoS2 oxide/MgCl2 (ethoxide type)/TiCl4/TiBA: study of thermo-mechanical properties of system, Int. J. Network. Commun. 6 (2) (2019) 87–108, https://doi.org/10.22034/ijnc.2019.33520.
[82] R. Kotsilkova, I. Borovanska, P. Todorov, E. Ivanov, D. Menseidov, S. Chakraborty, C. Bhattacharjee, Tensile and surface mechanical properties of polyethersulphone (PES) and polyvinylidene fluoride (PVDF) membranes, J. Theor. Appl. Mech. 48 (2018) 85–99.
[83] Y. Mao, Q. Huang, B. Meng, K. Zhou, G. Liu, A. Gugliuzza, E. Drioli, W. Jin, Roughness-enhanced hydrophobic graphene oxide membrane for water desalination via membrane distillation, J. Membr. Sci. 611 (2020) 118364, https://doi.org/10.1016/j.memsci.2020.118364.
[84] C. Li, X. Li, X. Du, T. Tong, T.Y. Cath, J. Lee, Antiwetting and antifouling Janus membrane for desalination of saline oily wastewater by membrane distillation, ACS Appl. Mater. Interfaces 11 (20) (2019) 18456–18465, https://doi.org/10.1021/acsami.9b04212.
[85] S. Mansour, A. Giwa, S.W. Hasan, Novel graphene nanoplatelets-coated polyethylene membrane for the treatment of reject brine by pilot-scale direct contact membrane distillation: an optimization study, Desalination 441 (2018) 9–20, https://doi.org/10.1016/j.desal.2018.04.026.
[86] W. Intrchom, S. Roy, M.S. Humoud, S. Mitra, Immobilization of graphene oxide on the permeate side of a membrane distillation membrane to enhance flux, Membranes 8 (3) (2018) 63.
[87] M. Bhadra, S. Roy, S. Mitra, Desalination across a graphene oxide membrane via direct contact membrane distillation, Desalination 378 (2016) 37–43, https://doi.org/10.1016/j.desal.2015.09.026.
[88] D.H. Seo, S. Pineda, Y.C. Woo, M. Xie, A.T. Murdock, E.Y.M. Ang, Y. Jiao, M. J. Park, S.I. Lim, M. Lawn, F.F. Borghi, Z.J. Han, S. Gray, G. Millar, A. Du, H. K. Shon, T.Y. Ng, K. Ostrikov, Anti-fouling graphene-based membranes for effective water desalination, Nat. Commun. 9 (1) (2018) 683, https://doi.org/10.1038/s41467-018-02871-3.
[89] Y. Jia, G. Xu, X. An, Y. Hu, Robust reduced graphene oxide composite membranes for enhanced anti-wetting property in membrane distillation, Desalination 526 (2022) 115549, https://doi.org/10.1016/j.desal.2022.115549.